24th COBEM - 2017

24th ABCM International Congress of Mechanical Engineering
December 3-8, 2017, Curitiba, PR, Brazil

COBEM-2017-1409
NATURAL CONVECTION OF VISCOPLASTIC FLUIDS IN A SQUARE ENCLOSURE

Daniel Dall'Onder dos Santos
Luiz Paulo Borges Miranda
Federal University of Uberlândia
dallonder@ufu.br
luizpaulobmiranda@hotmail.com

Abstract. *This work describes the numerical simulation of natural convection heat transfer of viscoplastic fluids in a two-dimensional square enclosure. The mechanical model is defined by the mass, momentum and energy balance equations coupled to constitutive equations to model the viscoplastic fluid behavior, namely the regularized Bingham and SMD equations. This modeling is approximated by a stabilized multi-field Galerkin finite element methodology, having as primal variables the extra-stress, velocity, pressure and temperature fields. In this way, the compatibility conditions between the extra-stress-velocity and pressure-velocity finite element subspaces are violated, allowing the use of equal-order finite element interpolations. In the performed numerical simulations, the fluid rheological parameters are varied in order to evaluate their influence on the heat transfer through the geometry. The numerical results are in accordance with the related literature.*
Keywords: *SMD viscoplastic model, natural convection, heat transfer on non-Newtonian fluids, Galerkin least-squares approximation*

1. INTRODUCTION

Non-Newtonian fluid flows are commonly found in industrial processes, especially those involved in the oil industry, cosmetics and food processing, and due their unique properties, it is important to study and understand their behavior. Among all the non-Newtonian effects, the viscoplastic behavior stand out: these fluids are characterized by a solid-like behavior at low stresses and a fluid-like behavior above a yield stress. The Bingham model and the Herschel-Bulkley model are frequently used to account for this behavior.

The natural convection heat transfer in viscoplastic systems differs significantly from that in Newtonian fluids or in purely viscous fluids without a yield stress: the coexistence of the fluid-like (yielded) and solid-like (unyielded) regions in the flow domain depending upon the local stress levels affect the properties of the flow and the heat transfer too: in the unyielded portions the heat transfer occurs mainly by conduction whereas convection is limited to the yielded fluid-like parts of the system.

The dimensionless numbers play an essential role in the process of understanding the heat transfer behavior. As they are able to condense information about the physics of the problem, they are the natural choice for several studies that look for correlations between then. Turan *et al.* (2011) simulated a two-dimensional steady-state natural convection in rectangular enclosures with differentially heated side walls in a range of different aspect ratios of the enclosure, a range of Rayleigh numbers, and a range of Bingham numbers too. Raja *et al.* (2015) investigated the flow of a Bingham plastic fluid past a two-dimensional heated flat plate over a range of Reynolds numbers, Prandtl numbers, and Bingham numbers. Nirmalkar *et al.* (2014) solved numerically the equations of motion and energy for the laminar free convection heat transfer from a horizontal heated cylinder to Bingham plastic fluids over the range of conditions as: Rayleigh number, Prandtl number, and Bingham number. Shyam and Chhabra (2013) have developed a numerical solution for the momentum and heat transfer characteristics of a heated cylinder of square cross-section immersed in a streaming Bingham plastic medium, with the conditions imposed as: the plastic Reynolds number, the Prandtl number, and the Bingham number.

From the experimental point of view, Davaille *et al.* (2013) performed experiments on the development of thermal plumes out of a localized heat source in a viscoplastic fluid. According to a dimensionless number that compares the thermally-induced stress to the yield stress, the authors observed three different flow regimes: no convection, a small-scale convection region appearing at the vicinity of the heater and the development of a thermal plume. Temperature and velocity field measurements show that a plug flow develops within the thermal plume. Karimfazli *et al.* (2016) studied an analogous problem both analytically and computationally for an ideal yield stress fluid, using the Bingham model, which is initially stationary in a locally heated rectangular tank. For strongly convecting flows (larger Ra numbers) the authors observed an increasing number of distinct plume heads and a tendency for plumes to develop as short-lived

pulses. The fluid yield stress plays a multifaceted role as it affects the plume temperature, size and velocity through different mechanisms.

As all this studies are analyzing a non-Newtonian fluid flow with heat transfer, it is natural to search for a correlation between all the dimensionless parameters and the average Nusselt number of the flow. The Nusselt number represent the relation between the heat transfer by convection and the heat transfer by conduction. As already stated, it is possible for a viscoplastic fluid flow to have unyielded regions, where conduction is the main heat transfer mechanism. This way, the yielded-unyielded proportion has a direct impact in the mean Nusselt number of the system: as shown by all the studies mentioned above, with the increase of the Bingham number, the unyielded areas tends to increase, and the heat transfer by convection tends to decrease, leading to lower Nusselt numbers. If the Bingham number tends to infinite, all the flow will be completely unyielded, thus the heat transfer will be performed purely by conduction and the average Nusselt will be equal to the unity.

Besides this correlation between the Bingham number and the Nusselt number, the mentioned studies also highlight a positive dependence of the Nusselt number with the Reynolds number and the Prandtl number. Some of these articles also have analyzed the influence of a geometrical factor, the aspect ratio of a rectangular enclosure, for example. In this case, they have found that the geometry that maximize the average Nusselt number is function of the combination of the dimensionless factors, like the Bingham number and the Prandtl number, for example. To validate their results and systems, Turan *et al.* (2011) have compared the obtained results with the results found in the literature. Another strategy to validate their results is to compare the results obtained with the particular case of the Bingham number equal to zero – this condition can be seen as purely Newtonian fluid, and more data is available in the literature to validate the results.

Although the use of dimensionless numbers is unquestionable, the choice of the set of dimensionless numbers in each problem is a matter of discussion. Thompson and Soares (2016) discussed about how the use of only one dimensionless number, like Prandtl number or Bingham number, can lead to ambiguous conclusions: as the yield stress is responsible for viscous and plastic effects, one is not isolating the plastic effect of the yield stress.

This work aims to perform numerical simulations of natural convection heat transfer of viscoplastic fluids in a two-dimensional square enclosure. The mass, momentum and energy balance equations are coupled to constitutive equations to model the viscoplastic fluid behavior, namely the regularized Bingham and SMD equations. This modeling is approximated by a stabilized multi-field Galerkin finite element methodology which has as primal variables the extra-stress, velocity, pressure and temperature fields. The stability parameters allows the the use of equal-order finite element interpolations for all variables, in this way, circumventing the compatibility conditions between the extra-stress-velocity and pressure-velocity finite element subspaces. In the performed numerical simulations, the fluid and flow dimensionless parameters are varied in order to evaluate their influence on the heat transfer through the geometry. The results are in accordance with the related literature.

2. MECHANICAL MODEL

The mechanical model employed in this work to describe non-isothermal and incompressible flows of viscoplastic fluids was formed by coupling the mass, momentum and energy balance equations with two different constitutive equations – the regularized Bingham model (Papanastasiou, 1987) and the modified SMD model (de Souza Mendes and Dutra, 2004),(de Souza Mendes, 2009):

$$\begin{aligned}
\eta_{Bingham-Reg}(\dot{\gamma}) &= \left(1 - exp\left(-m\dot{\gamma}\right)\right)\frac{\tau_0}{\dot{\gamma}} + \mu_p \\
\eta_{SMD-Modif}(\dot{\gamma}) &= \left(1 - exp\left(-\frac{\eta_0}{\tau_0}\dot{\gamma}\right)\right)\left(\frac{\tau_0}{\dot{\gamma}} + K\dot{\gamma}^{n-1}\right) + \eta_\infty
\end{aligned} \tag{1}$$

where μ_p is the viscous parameter of the Bingham material, m is a numerical parameter, τ_0 is the yield stress limit of the material, K is the consistency index, η_0 and η_∞ are, respectively, the viscosities for very low and high values of the shear rate; n is the power-law index, which controls the shear-thinning and shear-thickening of the viscosity when the material starts to flow. The SMD model has a qualitative behavior observed for most viscoplastic liquids of interest: a high-viscosity plateau at low shear rates, followed by a sharp drop of the viscosity level leading to a power-law region and a low-viscosity plateau for higher shear rate values – this last part is added to avoid a zero viscosity non-physical behavior. Subjecting the system to the appropriate velocity, stress and temperature boundary conditions, it becomes

$$\begin{aligned}
&\rho(\nabla\mathbf{u})\mathbf{u} = -\nabla p + \operatorname{div}\boldsymbol{\tau} + \rho\mathbf{g}\beta(T - T_{ref}) && \text{in } \Omega \\
&\boldsymbol{\tau} = 2\eta(\dot{\gamma})\mathbf{D}(\mathbf{u}) && \text{in } \Omega \\
&\operatorname{div}\mathbf{u} = 0 && \text{in } \Omega \\
&\rho c_p(\nabla T)\mathbf{u} = \kappa\nabla^2 T + q''' && \text{in } \Omega \\
&\mathbf{u} = \mathbf{u}_g && \text{over } \Gamma_g^{\mathbf{u}}
\end{aligned} \tag{2}$$

$$\begin{aligned}
&\boldsymbol{\tau} = \boldsymbol{\tau}_g && \text{over } \Gamma_g^{\boldsymbol{\tau}} \\
&T = T_g && \text{over } \Gamma_g^{T} \\
&(-p\mathbf{I} + \boldsymbol{\tau})\mathbf{n} = \mathbf{t}_h && \text{over } \Gamma_h
\end{aligned}$$

where $\mathbf{u}$ is the velocity vector, p the hydrostatic pressure, $\mathbf{D}$ the strain rate tensor, $\boldsymbol{\tau}$ is the extra-stress tensor, β is the volumetric thermal expansion coefficient, T the temperature, and T_{ref} a reference temperature, $\mathbf{g}$ the gravity vector; ρ, c_p, and κ are, respectively, the fluid density, specific heat, and thermal conductivity; η is the non-Newtonian viscosity, function of the shear-rate-dependent defined as $\dot{\gamma} = (2tr\mathbf{D}^2)^{1/2}$. $\mathbf{t}_h$ is the stress vector. $\mathbf{u}_g$, $\boldsymbol{\tau}_g$, and T_g are the imposed velocity, extra-stress, and temperature boundary conditions, respectively. It is important to mention that heat source effects are neglected in this work, although their modeling is presented in Eq. (2).

2.1 Numerical approximation

The Galerkin least-squares approximation for the boundary value problem defined on Eq. (2) can be written as: given the appropriate Dirichlet and Neumman boundary conditions, find the set $\boldsymbol{\tau}^h, \mathbf{u}^h, p^h, T^h \in \boldsymbol{\Sigma}^h, \mathbf{V}^h, P^h, \Theta^h$ such that

$$B(\boldsymbol{\tau}^h, \mathbf{u}^h, p^h, T^h; \mathbf{S}^h, \mathbf{v}^h, q^h, \psi^h) = F(\mathbf{S}^h, \mathbf{v}^h, q^h, \psi^h) \; \forall \; (\mathbf{S}^h, \mathbf{v}^h, q^h, \psi^h) \in \boldsymbol{\Sigma}^h \times \mathbf{V}^h \times P^h \times \Theta^h \tag{3}$$

with

$$\begin{aligned}
B(\boldsymbol{\tau}^h, \mathbf{u}^h, p^h, T^h; \mathbf{S}^h, \mathbf{v}^h, q^h, \psi^h) &= \int_\Omega \rho(\nabla \mathbf{u}^h)\mathbf{u}^h \cdot \mathbf{v}^h d\Omega \; - \int_\Omega p^h \mathrm{div}\mathbf{v}^h d\Omega \; + \int_\Omega \boldsymbol{\tau}^h \cdot \mathbf{D}(\mathbf{v}^h) d\Omega \\
&+ \int_\Omega \mathrm{div}\; \mathbf{u}^h q^h d\Omega \; + \epsilon \int_\Omega p^h q^h d\Omega \; + \int_\Omega \boldsymbol{\tau}^h \cdot \mathbf{S}^h d\Omega \; - 2\eta(\dot{\gamma}) \int_\Omega \mathbf{D}(\mathbf{u}^\mathbf{h}) \cdot \mathbf{D}(\mathbf{v}^h) d\Omega \\
&+ \sum_{K \in \Omega^h} \int_{\Omega_K} \delta_{GLS}(\mathrm{Re}_K) \mathrm{div}\; \mathbf{v}^h \; \mathrm{div}\; \mathbf{u}^h d\Omega \; + \int_\Omega \rho c_p (\nabla T^h)\mathbf{u}^h \psi^h d\Omega \; + \int_\Omega \kappa \nabla T^h \cdot \nabla \psi^h d\Omega \\
&+ \sum_{K \in \Omega^h} \int_{\Omega_K} \alpha(\mathrm{Re}_K) \left(\rho(\nabla \mathbf{u}^h)\mathbf{u}^h + \nabla p^h - \mathrm{div}\; \boldsymbol{\tau}^h\right) \cdot \left(\rho(\nabla \mathbf{v}^h)\mathbf{u}^h + \nabla q^h - \mathrm{div}\; \mathbf{S}^h\right) d\Omega \\
&+ \beta_{GLS} \int_\Omega \left(\boldsymbol{\tau}^h \; - 2\eta(\dot{\gamma})\mathbf{D}(\mathbf{u}^h)\right) \cdot \left(\mathbf{S}^h \; - 2\eta(\dot{\gamma})\mathbf{D}(\mathbf{v}^h)\right) d\Omega \\
&+ \sum_{K \in \Omega^h} \int_{\Omega_K} \xi_{GLS}(Pe_K) \left(\rho c_p(\nabla T^h)\mathbf{u}^h - \kappa \nabla^2 T^h\right) \left(\rho c_p(\nabla \psi^h)\mathbf{u}^h - \kappa \nabla^2 \psi^h\right)
\end{aligned} \tag{4}$$

and

$$\begin{aligned}
F(\mathbf{S}^h, \mathbf{v}^h, q^h, \psi^h) &= \int_\Omega \rho\beta(T^h - T_{ref})\mathbf{g} \cdot \mathbf{v}^h d\Omega + \int_\Omega q''' \psi^h d\Omega + \int_{\Gamma_h} \mathbf{t}_h \cdot \mathbf{v}^h d\Gamma \\
&+ \sum_{K \in \Omega^h} \int_{\Omega_K} \alpha(\mathrm{Re}_K)\rho\beta(T^h - T_{ref})\mathbf{g} \cdot \left(\rho(\nabla \mathbf{v}^h)\mathbf{u}^h + \nabla q^h - \mathrm{div}\; \mathbf{S}^h\right) d\Omega \\
&+ \sum_{K \in \Omega^h} \int_{\Omega_K} \xi_{GLS}(Pe_K) q''' \left(\rho c_p(\nabla \psi^h)\mathbf{u}^h - \kappa \nabla^2 \psi^h\right)
\end{aligned} \tag{5}$$

where $\epsilon << 1$. β_{GLS} is a positive arbitrary numerical constant set according to the error estimate introduced in Behr *et al.* (1993) – in this work it was used the value 0.5. The mesh Reynolds and Péclet numbers, Re_K e Pe_K respectively and the stability parameters $\alpha_{GLS}(Re_K)$, $\delta_{GLS}(Re_K)$ and $\xi_{GLS}(Pe_K)$ are defined as in Franca *et al.* (1992), Franca and

Frey (1992), and Behr *et al.* (1993),

$$
\begin{aligned}
&\alpha_{GLS}(\mathrm{Re}_K) = \frac{h_K}{2\left|\mathbf{u}^h\right|_p}\,\zeta_1(\mathrm{Re}_K) \quad , \quad \delta_{GLS}(\mathrm{Re}_K) = \lambda_d \left|\mathbf{u}^h\right|_p h_K \zeta_1(\mathrm{Re}_K) \\
&\mathrm{Re}_K = \frac{\rho\, h_K \left|\mathbf{u}^h\right|_p m_k}{4\,\eta_{eq}(\dot{\gamma})} \quad , \quad \zeta_1(\mathrm{Re}_K) = \begin{cases} 0, & \text{if } 0 < \mathrm{Re}_K < 1 \\ 1, & \text{if } \mathrm{Re}_K \geq 1 \end{cases} \\
&\xi_{GLS}(\mathrm{Pe}_K) = \frac{h_K}{2\left|\mathbf{u}^h\right|_p}\,\zeta_2(\mathrm{Re}_K) \\
&\mathrm{Pe}_K = \frac{h_K \left|\mathbf{u}^h\right|_p m_k}{2\,\kappa} \quad , \quad \zeta_2(\mathrm{Pe}_K) = \begin{cases} 0, & \text{if } 0 < \mathrm{Pe}_K < 1 \\ 1, & \text{if } \mathrm{Pe}_K \geq 1 \end{cases} \\
&\left|\mathbf{u}^h\right|_p = \begin{cases} \left(\sum_{i=1}^{N} \left|\mathbf{u}^h\right|^p\right)^{1/p}, & \text{if } 1 \leq p < \infty \\ \max_{i=1,N} \left|u_i^h\right| \quad , & \text{if } p = \infty \end{cases} \\
&m_k = \min\{1/3, 2C_k\} \quad , \quad C_k \sum_{K \in \Omega^h} h_K^2 \left\|\mathrm{div}\, \mathbf{S}^h\right\|_{0,K}^2 \geq \left\|\mathbf{S}^h\right\|_K^2 \quad \forall \quad \mathbf{S}^h \in \mathbf{\Sigma}^h
\end{aligned}
\tag{6}
$$

where λ_d is a positive paramenter and h_K is the mesh element size. It is important to mention that when α_{GLS}, β_{GLS}, δ_{GLS} and ξ_{GLS} tend to zero, the classical Galerkin formulation is obtained. The mesh Reynolds number employed is based in Johnson (1987), and was modified (parameter m_k) to consider the degree of the interpolation function.

3. RESULTS

The multi-field Galerkin least-squares approximation shown in the previous section is employed to simulate natural convection heat transfer inside a square enclosure. Figure 1 shows the geometry and the mesh employed in the simulations. After a mesh independence test procedure, based on an acceptable error of 3% on the temperature profile at the cavity horizontal mid-plane, the computational domain was partitioned by 2,500 equal-order Lagrangian bi-linear (Q1) finite elements, rendering a total of 18,207 degrees-of-freedom. The dimensionless mesh size, $h_K^* = hK/H$, is uniform and equal to 0.02. Is worthwhile to mention that the representation of the unyielded regions is hampered by using such a h_K^*. On the other hand, the time consumed by the numerical computations is low when compared to the more refined meshes.

The velocity boundary conditions employed are impermeability and non-slip over the cavity walls. The upper and lower walls are considered thermally insulated, while the left and right walls have prescribed temperatures according to Fig. 1a.

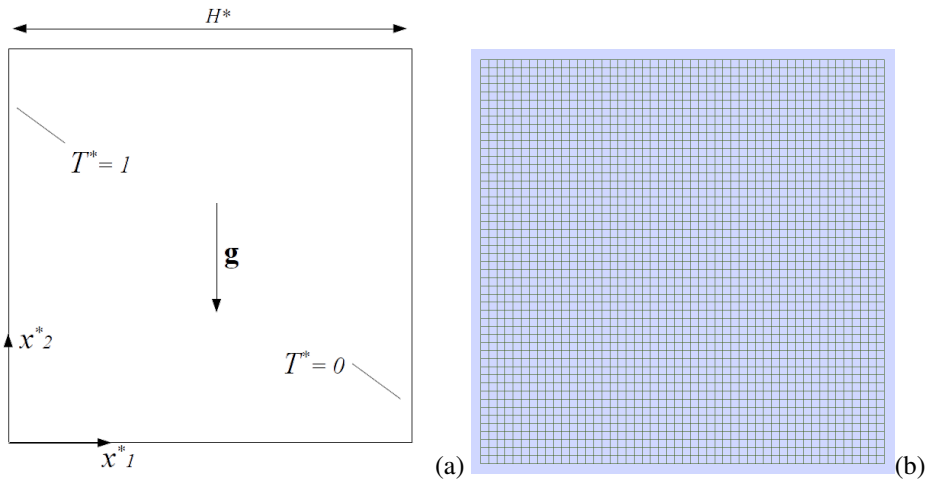

Figure 1. The geometry. (a) Boundary conditions; (b) Employed mesh.

3.1 Results using the regularized Bingham model

The results obtained using the Bingham model, in order to validate the numerical methodology with results found in the literature, are shown in Figs. 2 and 3. The dimensional quantities involved, namely the Rayleigh, Bingham and Prandtl numbers are calculated as suggested by Turan *et al.* (2010) (Ra_T, Bn_T and Pr_T). The results for vertical velocity and temperature profiles at the cavity horizontal mid-plane show a good agreement for $Pr_T = 7$, ranging the Rayleigh

number from 10^3 to 10^5 with $Bn_T = 0.5$ and ranging the Bingham number from 0 (Newtonian) to 1.0 with $Ra_T = 10^4$.

For $Ra_T = 10^4$, Pr_T=7 and Bn_T=0.5, the average Nusselt number at the left wall is 1.519, while Turan *et al.* (2010) found a value of 1.5248; for the maximum vertical velocity at the horizontal mid-plane ($V^*_{max,T}$), the value found in this work is 8.9474, while Turan *et al.* (2010) found a value of 8.949 for they more refined mesh.

As mentioned before, as the Bingham number is increased, the fluid unyielded regions (obtained with the $\tau > \tau_0$ criterion) become larger (Fig. 4) and the convection heat transfer is rapidly diminished (Tab. 1). The fluid begins to present the solid-like behavior: for instance, there is no significant fluid motion for $Bn_T = 1.5$, as illustrated by the temperature field (Fig. 5). For this case, the temperature distribution is very similar of the one obtained for a solid subjected to the same temperature boundary conditions.

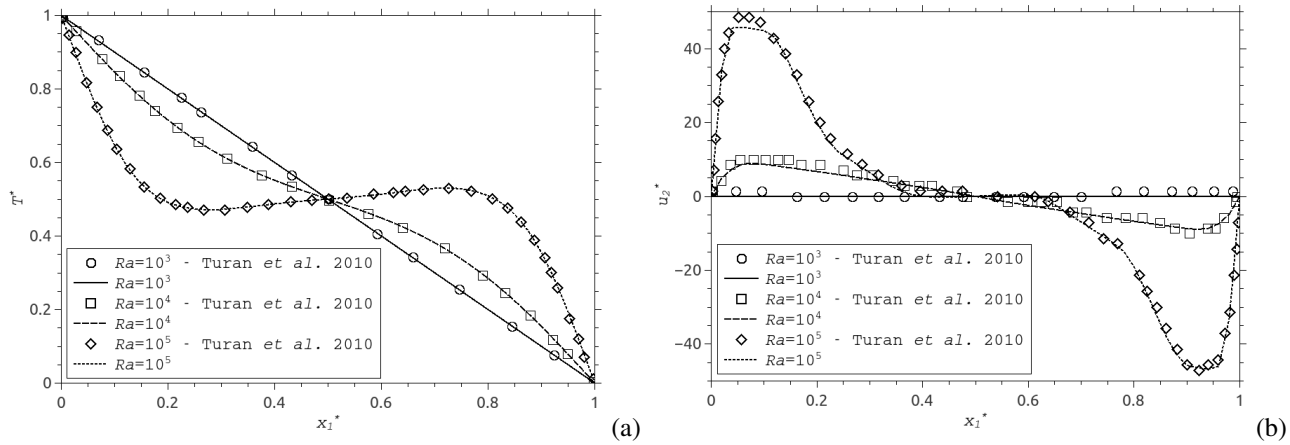

(a) (b)

Figure 2. Comparison with Turan *et al.* (2010), for the Rayleigh number variation. Profiles at the cavity horizontal mid-plane: (a) Temperature; (b) Vertical velocity.

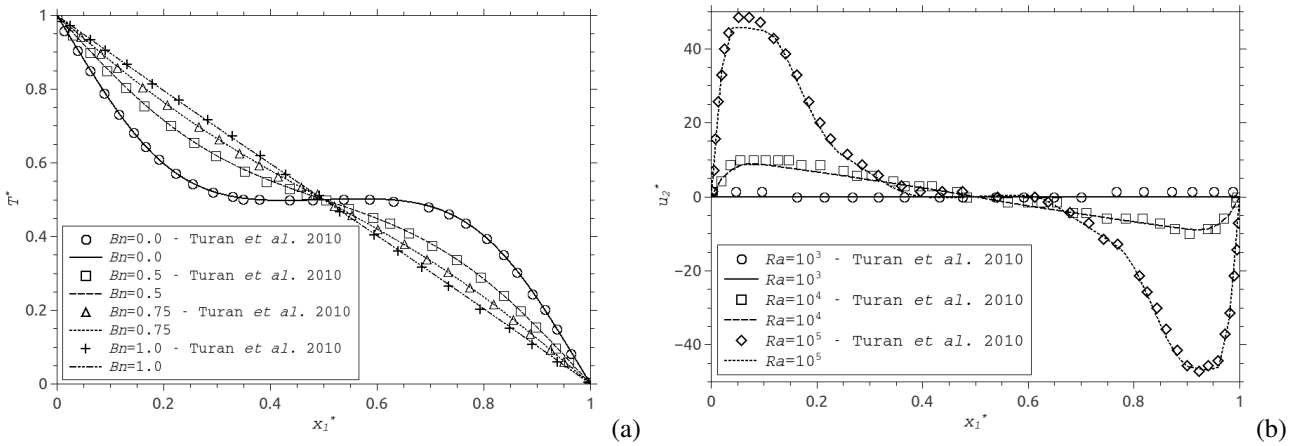

(a) (b)

Figure 3. Comparison with Turan *et al.* (2010), for the Bingham number variation. Profiles at the cavity horizontal mid-plane: (a) Temperature; (b) Vertical velocity.

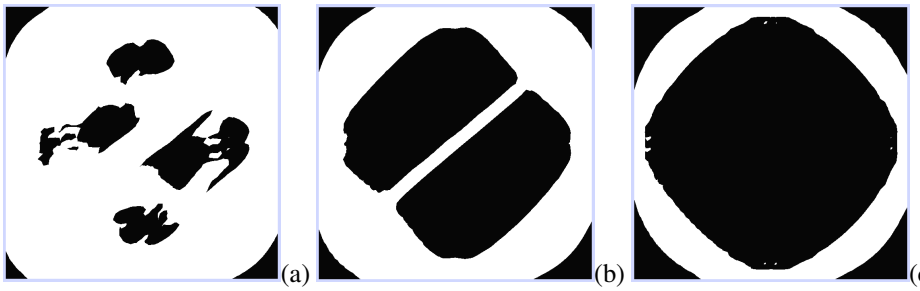

(a) (b) (c)

Figure 4. Bingham number variation: unyielded regions. (a) Bn_T=0.5; (b) Bn_T=0.75; (c) Bn_T=1.0.

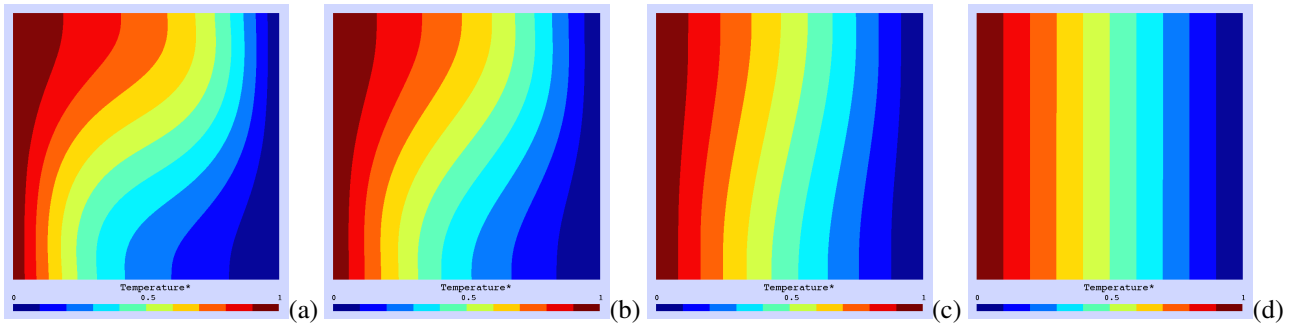

(a) (b) (c) (d)

Figure 5. Bingham number variation: temperature field. (a) Bn_T=0.5; (b) Bn_T=0.75; (c) Bn_T=1.0; (d) Bn_T=1.5.

Table 1. Average Nusselt number ranging the Bingham number from 0.0 to 1.5.

Bn_T	0.0	0.5	0.75	1.0	1.5
Nu_H	2.267	1.519	1.210	1.024	1.000

3.2 Results using the SMD model

In order to evaluate the effect of the power-law index on the average Nusselt number and over the flow unyielded regions, the following quantities were employed (Thompson and Soares, 2016):

$$\tau_c = \rho g \beta \Delta T L \qquad U_c = L\left(\frac{\tau_c - \tau_0}{K}\right)^{1/n} \qquad \eta^* = \frac{\eta}{\eta_c} = \frac{\eta}{\frac{\tau_0}{U_c/L} + K(U_c/L)^{n-1}} \qquad Pl = \frac{\tau_0}{\tau_0 + K(U_c/L)^n}$$
$$Ra = \left(\frac{K(U_c/L)^n}{\tau_0 + K(U_c/L)^n}\right)\frac{\rho g \beta \Delta T L^3}{K(U_c/L)^{n-1}\alpha} \qquad \frac{1}{Pr} = \left(\frac{K(U_c/L)^n}{\tau_0 + K(U_c/L)^n}\right)\frac{\rho\alpha}{K(U_c/L)^{n-1}} \tag{7}$$

where τ_c is the characteristic stress of the natural convection problem. The stresses, induced by the temperature difference, must overcome the yield stress in order to actually induce motion (Thompson and Soares, 2016). U_c is the characteristic velocity obtained from the driving potential that arises from the difference between τ_c and τ_0. Pl is the plastic number, a normalized quantity that indicates how plastic the material is. Ra and Pr are respectively the Rayleigh and Prandtl numbers obtained with the rationale shown by Thompson and Soares (2016).

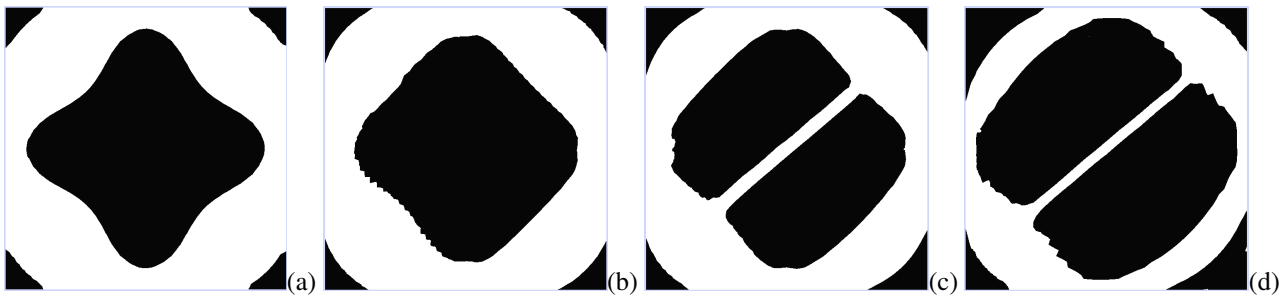

(a) (b) (c) (d)

Figure 6. Power-law index variation: unyielded regions. (a) n=0.5; (b) n=0.75; (c) n=1.0; (d) n=1.5.

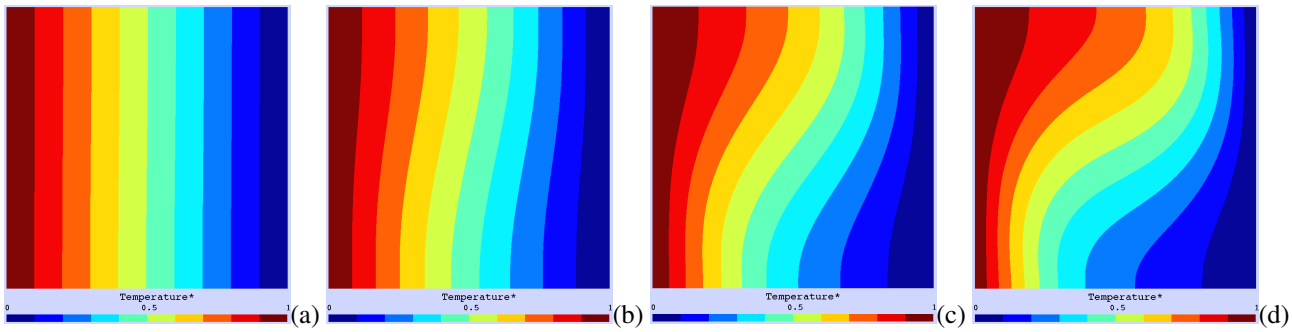

(a) (b) (c) (d)

Figure 7. Power-law index variation: temperature field. (a) n=0.5; (b) n=0.75; (c) n=1.0; (d) n=1.5.

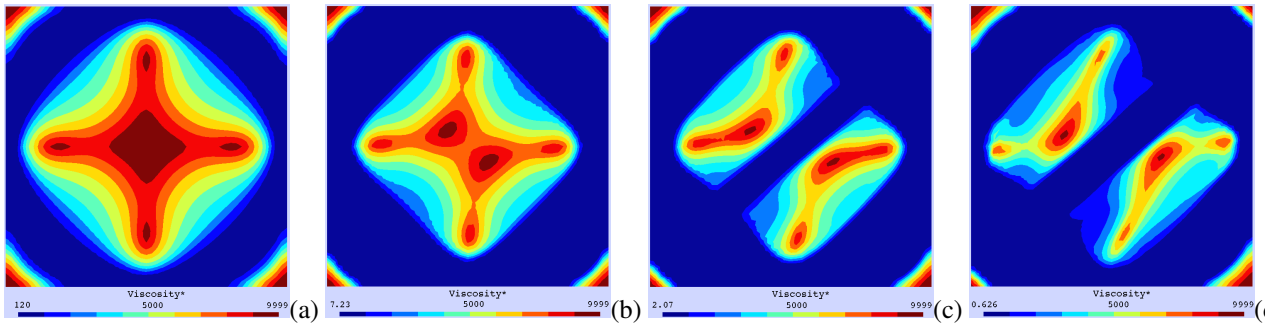

(a) (b) (c) (d)

Figure 8. Power-law index variation: viscosity field. (a) n=0.5; (b) n=0.75; (c) n=1.0; (d) n=1.5.

Figure 6 shows the flow unyielded regions for Pl=0.0198, Ra=9800 and Pr=7.14, using $\eta_0^* = 10000$ and $\eta_\infty^* = 0.01$, ranging the n index. Is worthwile to mention that the dimensional quantities of the SMD model were varied in orther to perform all the numerical simulations subjecting the flow to the same driving potential (τ_c) and dimensionless parameters. This, in fact, lead to a controversial result. There is a growth of the unyielded regions as the power-law index is increased, but the viscosity field (Fig. 8) shows that the regions subjected to the higher viscosity levels are smaller. The vertical velocity profiles at the cavity horizontal midplane, for each power-law index simulated, is shown in Fig. 9a and make clear the increase of u_2^* with n. This behavior intensifies the heat transfer between the cavity walls, as shown by Fig. 7 and by the growth of the average Nusselt number over the left wall (Fig. 9b).

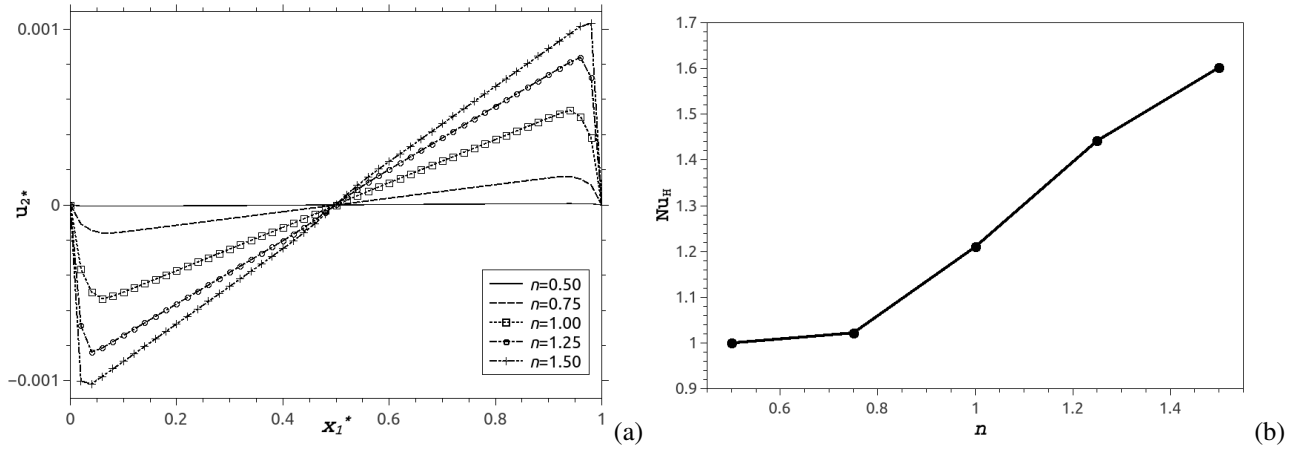

(a) (b)

Figure 9. Power-law index variation. (a) Vertical velocity profiles. (b) Average Nusselt number.

4. CONCLUSIONS

The results obtained with the Bingham model presented in this work showed a very good agreement with the related literature. The numerical approximation of the mechanical model was able to produce stable results even employing a coarse mesh (50 x 50 elements) – although the representation of the unyielded regions is somewhat compromised. The results employing the SMD model, capable to model the shear thinning and shear thickening effects on viscoplastic fluids, shown a contraditory effect: while the flow unyielded regions are apparently increased with the power-law index, the heat transfer inside the cavity is also increased. This behavior is due to the lower viscosity levels experienced by the fluid once the same dimensionless parameters are kept constant.

5. ACKNOWLEDGEMENTS

The authors acknowledge FAPEMIG and the Faculty of Mechanical Engineering (FEMEC/UFU) for the financial support.

6. REFERENCES

Behr, A.M., Franca, L.P. and Tezduyar, T.E., 1993. "Stabilized finite element methods for the velocity-pressure-stress formulation of incompressible flows". *Computer Methods Appl. Mech. Eng.*, Vol. 104, pp. 31–48.

Davaille, A., Gueslin, B., Massmeyer, A. and Di Giuseppe, E., 2013. "Thermal instabilities in a yield stress fluid: Existence and morphology". *Journal of Non-Newtonian Fluid Mechanics*, Vol. 193, pp. 144–153.

de Souza Mendes, P.R., 2009. "Modeling the thixotropic behavior of structured fluids". *Journal of Non-Newtonian Fluid Mechanics*, Vol. 164, pp. 66–75.

de Souza Mendes, P.R. and Dutra, E.S.S., 2004. "Viscosity function for yield-stress liquids". *Applied Rheology*, Vol. 14, pp. 296–302.

Franca, L.P. and Frey, S.L., 1992. "Stabilized finite element methods: II. the incompressible Navier-Stokes equations". *Comput. Methods. Appl. Mech. Eng.*, Vol. 99, pp. 209–233.

Franca, L.P., Frey, S.L. and Hughes, T.J.R., 1992. "Stabilized finite element methods: I. Application to the advective-diffusive model". *Comput. Methods. Appl. Mech. Eng.*, Vol. 95, pp. 253–276.

Johnson, C., 1987. *Numerical solution of partial differential equations by the finite element method*. Cambridge University Press.

Karimfazli, E., Frigaard, I.A. and Wachs, A., 2016. "Thermal plumes in viscoplastic fluids: flow onset and development". *Journal of Fluid Mechanics*, Vol. 787, pp. 474–507.

Nirmalkar, N., Bose, A. and Chhabra, R.P., 2014. "Free convection from a heated circular cylinder in Bingham plastic fluids". *International Journal of Thermal Sciences*, Vol. 83, pp. 33–44.

Papanastasiou, T.C., 1987. "Flow of materials with yield". *Journal of Rheology*, Vol. 31, pp. 385–404.

Raja, A.H., Patel, S.A. and Chhabra, R.P., 2015. "Laminar forced convection heat transfer from a two-dimensional transverse plate in Bingham plastic fluids". *International Journal of Heat and Mass Transfer*, Vol. 83, pp. 690–709.

Shyam, R. and Chhabra, R.P., 2013. "Effect of prandtl number on heat transfer from tandem square cylinders immersed in power-law fluids in the low Reynolds number regime". *International Journal of Heat and Mass Transfer*, Vol. 57, pp. 742–755.

Thompson, R.L. and Soares, E.J., 2016. "Viscoplastic dimensionless numbers". *Journal of Non-Newtonian Fluid Mechanics*, Vol. 238, pp. 57–64.

Turan, O., Chakraborty, N. and R. J. Poole, N., 2010. "Laminar natural convection of Bingham fluids in a square enclosure with differentially heated side walls". *Journal of Non-Newtonian Fluid Mechanics*, Vol. 165, pp. 901–913.

Turan, O., Poole, R.J. and N. Chakraborty, N., 2011. "Aspect ratio effects in laminar natural convection of Bingham fluids in rectangular enclosures with differentially heated side walls". *Journal of Non-Newtonian Fluid Mechanics*, Vol. 166, pp. 208–230.

7. RESPONSIBILITY NOTICE

The authors are the only responsible for the printed material included in this paper.